ELSEVIER

Journal of Luminescence 96 (2002) 87–93

JOURNAL OF LUMINESCENCE

www.elsevier.com/locate/jlumin

Time-resolved luminescence of ZnS:Mn^{2+} nanocrystals

C. de Mello Donegá*[,1], A.A. Bol, A. Meijerink

Department of Physics and Chemistry of Condensed Matter, Debye Institute, Utrecht University, Princetonplein 1, P.O. Box 80000, 3508 TA Utrecht, The Netherlands

Received 25 April 2001; received in revised form 3 October 2001; accepted 3 October 2001

Abstract

Recently, Yu and co-workers reported the observation of hot luminescence for Mn^{2+} in 3.6 nm ZnS nanocrystals, implying that the phonon relaxation rates in nanocrystals were $\sim 10^6$ times lower than that in bulk materials. In order to verify this unexpected observation, we investigated the time-resolved spectroscopy of 4.5 nm ZnS:Mn^{2+} nanocrystals. Samples with two different Mn^{2+} concentrations were studied. In contradiction with the results reported by Yu and co-workers, no evidence of Mn^{2+} hot luminescence was found, regardless of the Mn^{2+} concentration, temperature (4.2–300 K), time delay (0.1–1000 μs), gate width (2–3000 μs), or excitation density (40–700 mJ/cm^2).

PACS: 71.55.Gs; 78.67.Bf; 78.47.+p; 78.55.Et

Keywords: ZnS:Mn^{2+} photoluminescence; Nanocrystals; Hot luminescence; Time-resolved luminescence

1. Introduction

Nanocrystalline semiconductors have attracted great interest over the past few years because their properties are remarkably different from bulk semiconductors. These differences arise from several phenomena (viz., quantum confinement of electrons and holes, surface effects, and geometrical confinement of phonons), which may play different roles depending on the investigated property [1–6]. The nanoparticle has a rather large number of atoms but its size is comparable with characteristic dimensions describing the behaviour of electrons and holes in semiconductors, thus creating an intermediate regime between molecules and bulk crystals [1–6]. Therefore, one can use materials with already desirable bulk properties and improve or tailor these properties by a judicious control of size and surface [1–6].

More recently, the optical properties of transition metal ion-doped semiconductor nanoparticles have attracted increasing interest, and many reports on new phenomena have appeared. One of the first such reports claimed that nanocrystalline ZnS:Mn^{2+} can yield simultaneously both a higher luminescence efficiency and a lifetime shortening from ms to ns, in comparison with bulk ZnS:Mn^{2+} [7], thus defining a new class of materials with a wide range of possible applications (e.g. plasma displays, sensors, lasers) [8]. To

*Corresponding author. Tel.: +31-30-2532226; fax: +31-30-2532403.

E-mail address: c.demellodonega@phys.uu.nl (C. de Mello Donegá).

[1] On leave from Depto. de Química Fundamental, Federal State University of Pernambuco, Recife, Brazil.

0022-2313/02/$ - see front matter
PII: S0022-2313(01)00418-5

explain these unexpected phenomena, Barghava and Gallagher [7,8] proposed that a strong hybridization between the s–p states of the ZnS host and the d states of the Mn^{2+} impurity should occur with decreasing particle sizes, leading to both a decrease in the spin-forbidden character of the $^4T_1$–$^6A_1$ emission transition of Mn^{2+} and a faster energy transfer between host and impurity, thus enhancing the efficiency of the radiative recombination at the Mn^{2+} ions and shortening its decay times. However, this explanation also implies that the position of the Mn^{2+} levels should shift due to the strong hybridization, what has never been observed [7–9].

These claims spurred many other publications, from different groups, reporting on the luminescent properties of Mn^{2+} doped nanocrystals [9–22]. Some groups reported the Mn^{2+} luminescence decay times to be in the ns range [10,12], whereas others observed it in the μs range [11,17]. It was later shown by two independent groups [16,18] that the fast decay luminescence observed in ZnS:Mn^{2+} nanocrystals was actually due to a ZnS defect-related emission, whereas the $^4T_1$–$^6A_1$ Mn^{2+} luminescence did not observably differ from that of bulk materials, showing a decay time of ca. 1.9 ms.

Recently, Mn^{2+} doped ZnS nanocrystals yielded yet another unexpected observation. In a study of the time-resolved emission spectra of 3.6 nm ZnS:Mn^{2+} nanocrystals embedded in polyvinylbutyral, Yu et al. [17] reported that, at short delay times, the $^4T_1$–$^6A_1$ luminescence band of Mn^{2+} consisted of two peaks, at the high- and low-energy sides of the expected peak position. In time, these two peaks shifted towards each other, finally merging into the expected single-peaked emission. These observations were interpreted as hot luminescence from higher vibrational states of the Mn^{2+} excited state [17], due to the localization of hot spots by the nanocrystals, resulting in enhanced phonon–phonon scattering and the consequent creation of a long-lived phonon reservoir (μs lifetime). Time-dependent band shape calculations performed shortly after by Anderson et al. [23] provided further support for this explanation, implying that the phonon relaxation rates for Mn^{2+} in the ZnS nanocrystals were 10^6 times lower than in bulk materials (i.e. $\sim 10^4$/s instead of $\sim 10^{10}$/s). In order to verify such a surprising possibility, we carried out time-resolved spectroscopic measurements on powder samples of 4.5 nm ZnS:Mn^{2+} nanocrystals. In this paper, we report on the results of our experiments, which, as will become clear below, provide no evidence of hot luminescence in ZnS:Mn^{2+} nanocrystals.

2. Experimental

Powder samples of polyphosphate stabilized ZnS:Mn^{2+} nanocrystals were prepared by an inorganic precipitation method [16,20]. A volume of 10 ml of a 1 M Na_2S aqueous solution was quickly injected into 90 ml of an aqueous solution containing 10 g of sodium polyphosphate, 10 mmol of $Zn(CH_3COO)_2 \cdot 2H_2O$ and 0.1 or 0.25 mmol of $Mn(CH_3COO)_2 \cdot 4H_2O$ (nominal concentration: 1 and 2.5 mol% Mn^{2+}), under vigorous stirring at room temperature. Immediately after the injection, an opaque white suspension formed and was kept under vigorous stirring for 15 min. The suspension was then centrifuged at 4000 rpm, rinsed with distilled water and ethanol, and subsequently dried overnight under vacuum, yielding a fine white powder.

The samples were characterized by diffuse reflectance spectroscopy (Perkin-Elmer Lambda 16) and X-ray powder diffraction (Philips PW1729 X-ray diffractometer, CuK_α, 3°/min). Luminescence spectra (emission and excitation) were recorded on a SPEX Fluorolog Spectrophotometer model F2002, equipped with two double grating 0.22 m SPEX monochromators and a 450 W Xe lamp as the excitation source.

Time-resolved spectroscopic measurements were performed by using the fourth harmonic of a Spectra Physics DCR 2 Q-Switched Nd:YAG laser as the excitation source ($\lambda_{exc} = 266$ nm, 10 ns pulse width, 10 Hz). An UV transmitting interference filter was placed before the sample to suppress any residual second harmonic light (532 nm). The excitation laser was focused onto the sample by a quartz lens and the luminescence was filtered through a 350 nm cut-off filter and focused into the slits of a Spex 1269 1.26 m monochromator. A

cooled (243 K) Hamamatsu R928P photomultiplier tube detected the dispersed light. A Stanford Research Systems SR400 2-channel Gated Photon Counter was used to analyse the signal, after amplification by a Stanford Research Systems SR445 300 MHz Amplifier. This set-up is equipped with an Oxford Instruments liquid Helium flow cryostat and a temperature controller, allowing for measurements down to 4.2 K. The laser power was measured at the second harmonic wavelength due to the higher sensitivity and faster response of the Joulemeter to 532 nm. The frequency doubling efficiency from 532 to 266 nm was 13%. The excitation densities were estimated for a laser spot size of $\sim 4\,mm^2$.

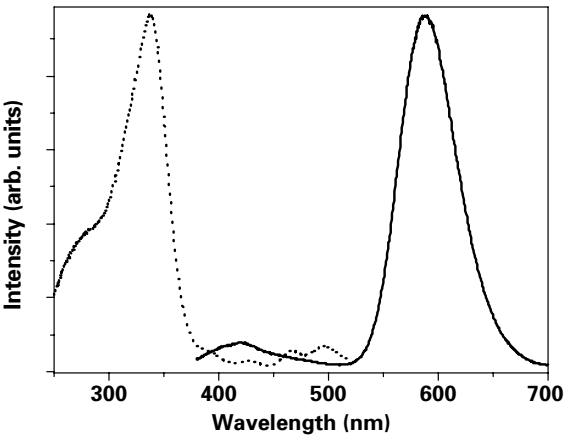

Fig. 1. The emission spectrum upon 300 nm excitation (solid line) and the excitation spectrum ($\lambda_{emission} = 590$ nm, dashed line) of the ZnS:Mn (2.5%) nanocrystalline powder sample, at room temperature.

3. Results and discussion

The diffuse reflectance spectra of both samples showed the expected strong ZnS absorption band in the UV. Absorption due to contaminations or sulphide-related colour centres were not observed. The X-ray diffraction patterns of the samples showed broad lines with maxima at the expected positions for the diffraction peaks of zinc blende ZnS (unit cell parameters: $Z = 4$; $a_0 = 5.410$ Å [24]). The mean particle diameters were calculated from the full-width at half-maximum of the peaks using the Scherrer formula [25], and were found to be 4.4 nm for the sample with a nominal Mn^{2+} concentration of 2.5 mol% (hereafter designated as ZnS:Mn (2.5%)) and 4.6 nm for the sample with a nominal Mn^{2+} concentration of 1 mol% (hereafter designated as ZnS:Mn (1%)). The actual Mn^{2+} concentration incorporated into the ZnS nanocrystals has not been determined in this work, but is expected to be about 10–50 times lower than the nominal concentration, based on values previously reported on the literature [19,20].

Fig. 1 presents the excitation and emission spectra of the ZnS:Mn (2.5%) nanocrystalline sample. The emission spectrum consists of a very intense broad band at 590 nm, ascribed to the $^4T_1$–$^6A_1$ transition of the Mn^{2+} ion, and a weaker broad band at about 425 nm, ascribed to radiative recombination at defects in the ZnS nanocrystals. The excitation spectrum of the Mn^{2+} luminescence shows a broad band with maximum at 330 nm, ascribed to the ZnS band gap transition, and several weak peaks from ~ 370 to ~ 530 nm, which can be attributed to intraconfigurational d–d transitions of the Mn^{2+} ions. The observation of the ZnS absorption band in the excitation spectrum of the Mn^{2+} luminescence shows that the Mn^{2+} ions are incorporated into the ZnS nanocrystals. The peak position of the ZnS band gap transition is not very different from the value observed for bulk samples (viz., 332 nm [26]), consistently with the estimated mean particle diameter. Considering that the exciton Bohr radius for ZnS zinc blende is 1.5 nm [27], particles with a 2.2 nm radius are in the weak quantum confinement regime, and thus cannot be expected to show any substantial shift in the absorption bands. The emission and excitation spectra of the ZnS:Mn (1%) nanocrystalline sample are similar to those of the ZnS:Mn (2.5%) sample presented above. As expected for a lower Mn^{2+} concentration, the Mn^{2+} d–d transitions are very weak in the excitation spectrum and the relative intensity for the Mn^{2+} related emission band is lower for ZnS:Mn (1%).

The room temperature time-resolved emission spectra of the ZnS:Mn (2.5%) nanocrystaline powder sample for a fixed 2 μs gate width and variable time delays are shown in Fig. 2. The gate

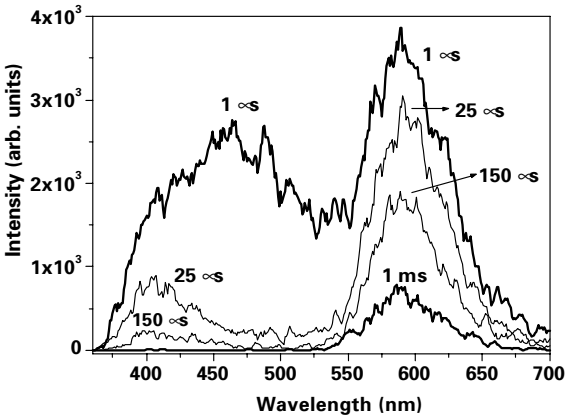

Fig. 2. Time-resolved emission spectra of the ZnS:Mn (2.5%) nanocrystalline powder sample, upon 266 nm excitation, with variable time delays (1, 25, 150, 1000 μs) and a fixed gate width of 2 μs. All spectra were recorded at room temperature. The excitation density was kept at 40 mJ/cm^2.

width was chosen so as to allow comparison with the data published by Yu et al. [17]. A time delay of 0.1 μs, not shown in Fig. 2, was also applied. As the time delay increases from 0.1 to 1000 μs, the Mn^{2+} emission band becomes more dominant in the spectrum, until it is the only observable emission. This is due to the fact that the decay time of the $^4T_1$–$^6A_1$ transition of the Mn^{2+} ion is in the ms range, whereas the defect-related ZnS emission decays in the sub-μs range [16]. The spectra also show that the ZnS emission at room temperature consists of at least two distinct bands, with maxima at 460 and 400 nm, the former decaying faster than the latter. In the time-resolved spectra with wider gate widths (viz., 10, 50, 200, 500, and 3000 μs), the 460 nm ZnS emission band is no longer observed, and the Mn^{2+} emission becomes more prominent as the gate width was increased. The spectra clearly show that the Mn^{2+} emission has a gaussian band shape with a maximum at 590 nm, regardless of the time delay and gate width, in contrast with the results published in Ref. [17]. The results for the ZnS:Mn (1%) sample are similar, apart from the higher relative intensity of the ZnS emission band.

The spectra shown in Fig. 2 were obtained while keeping the excitation density constant at 40 mJ/cm^2. We note that Yu et al. [17] investigated excitation densities ranging from 4 to 12 mJ/cm^2, and reported that the splitting of the Mn^{2+} band at short time delays was strongly power dependent, being already observable at 4 mJ/cm^2. Furthermore, the overall bandwidth was reported to decrease with increasing temperature, the intensity of the low-energy peak becoming lower than that of the high-energy peak [17]. Therefore, we investigated the power dependence of the time-resolved spectra of the ZnS:Mn (2.5%) sample at room temperature (Fig. 3) and at 4.2 K (Fig. 4). The time delay and gate width were kept constant at 1 and 2 μs, respectively. The excitation density ranged from 40 to 290 mJ/cm^2 at room temperature and from 40 to 700 mJ/cm^2 at 4.2 K. The actual power absorbed by the samples is hard to estimate, since the losses caused by scattering are difficult to evaluate quantitatively. These losses are likely to be substantial, especially for the measurements at 4.2 K, which had the extra scattering by the cryostat windows. Nevertheless, all the spectra are fully comparable since the instrumental conditions and alignment remained unchanged throughout the measurements. Furthermore, in both cases the excitation density was increased until the damage threshold of the samples was reached. Although only ZnS:Mn (2.5%) time-resolved spectra are shown here, the ZnS:Mn (1%) sample yielded similar results.

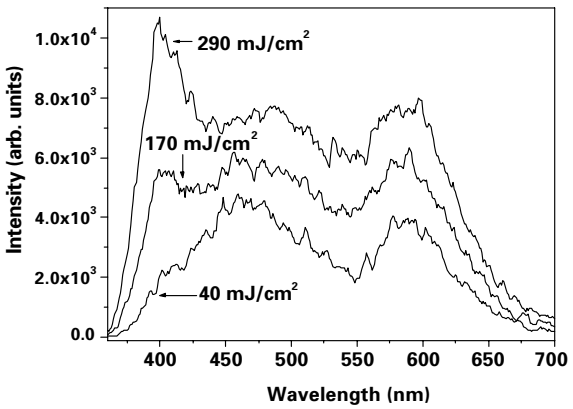

Fig. 3. Time-resolved emission spectra of the ZnS:Mn (2.5%) nanocrystalline powder sample, upon 266 nm excitation, with fixed time delay and gate width (1 and 2 μs, respectively), and variable excitation density. The labels give the excitation densities in mJ/cm^2. All spectra were recorded at room temperature.

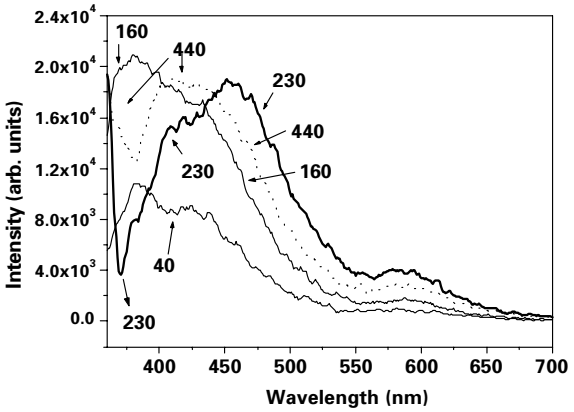

Fig. 4. Time-resolved emission spectra of the ZnS:Mn (2.5%) nanocrystalline powder sample, upon 266 nm excitation, with fixed time delay and gate width (1 and 2 μs, respectively), and variable excitation density. The labels give the excitation densities in mJ/cm^2. All spectra were recorded at 4.2 K.

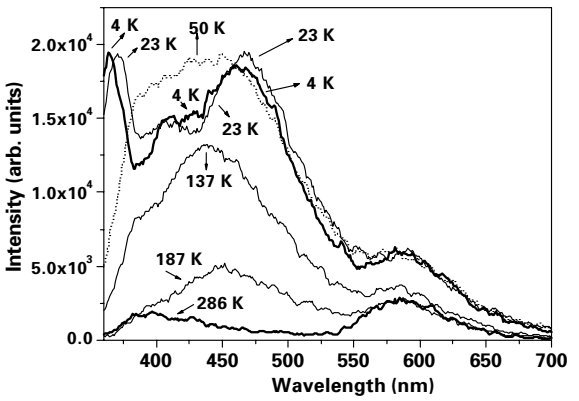

Fig. 5. Time-resolved emission spectra of the ZnS:Mn (2.5%) nanocrystalline powder sample, upon 266 nm excitation, with fixed time delay and gate width (1 and 2 μs, respectively), at different temperatures. The excitation density was kept at 290 mJ/cm^2.

The power and temperature dependences are much more pronounced for the ZnS emission than for the Mn^{2+} emission (Figs. 3 and 4). The position and shape of the Mn^{2+} $^4T_1$–$^6A_1$ emission band are independent of both power and temperature, while its intensity increases by just a factor 2 from 300 to 4.2 K. This weak temperature quenching of the Mn^{2+} luminescence under inter-band excitation in ZnS nanocrystals is consistent with the results reported before by Tanaka and Masumoto [22] for ZnS:Mn^{2+} nanocrystals embedded in polyvinyl alcohol films. In contrast, the intensity of the ZnS emission increases by 1 order of magnitude upon cooling to 4.2 K, with the concomitant appearance of new bands (Fig. 4). The bands observed at room temperature at 400 and 460 nm (Fig. 3) are no longer prominent features in the spectra at 4.2 K (Fig. 4). Moreover, the power dependence is not the same for different bands, so that the 400 nm band becomes the prominent feature in the room temperature spectra at higher excitation densities (Fig. 3). These different power dependences for different ZnS defect emissions are even more pronounced at 4.2 K (Fig. 4), with bands appearing, disappearing or shifting depending on the excitation densities. This process is fully reversible, provided the sample is not damaged.

The temperature dependence of the time-resolved emission spectra of the ZnS:Mn (2.5%) sample was investigated in more detail for a time delay of 1 μs and a gate width of 2 μs, keeping the excitation density constant at 290 mJ/cm^2 (Fig. 5). This value was chosen for further investigation, because it corresponds to the minimum excitation density at which drastic modifications occur. A very complex temperature-dependent behaviour is observed.

A detailed discussion of the temperature and power dependences of the ZnS-related emission bands is beyond the scope of this paper and requires more experimental results. Some of the emission bands observed in this work (viz., 350, 400 and 460 nm) have been previously reported by other groups (e.g. Ref. [10]) for ZnS:Mn^{2+} nanocrystals. The 350 nm band has been interpreted as due to near band gap emission, while the other two have been ascribed to radiative recombination at ZnS defects (traps) [10]. Similarly, the results presented above can be ascribed to a nonuniform distribution of electron and hole traps of different energy depths, and thus different quenching temperatures. At a given temperature, the increase in the excitation densities would cause the saturation of a portion of the trap distribution, thus allowing the emission of other traps to be observed. The increase in temperature favours nonradiative recombination at the traps, so at higher temperatures all ZnS-related emissions start

to quench, but at different rates for different traps. For example, the quenching temperature of the 400 nm defect emission is observed to be higher than that for the 350 or 460 nm emissions. An interesting observation is that at low temperatures and high-excitation densities, a strong emission around 350 nm is observed. As mentioned above, this emission is probably trapped exciton emission. At lower excitation densities, the fast trapping of the optically generated electrons and holes at defect sites competes with the exciton emission, preventing the observation of the near band edge exciton emission. At high excitation densities, the trap emission starts to saturate at low temperatures and exciton emission can then be observed. The power dependence of the emission spectra at room temperature is not easily explained and requires further investigations.

The results presented above are in contradiction with the data reported by Yu et al. [17], since the time-resolved spectra do not provide any evidence of Mn^{2+} hot luminescence in ZnS nanocrystals. The $^4T_1$–$^6A_1$ emission of Mn^{2+} in ZnS showed the expected "normal" band shape and a single maximum at 590 nm under all the experimental conditions investigated. Although finite size effects can be expected to cause phonon confinement, with consequences on nonradiative relaxation and optical dephasing processes [28], these effects will be restricted to the acoustic phonon modes, creating a low-frequency gap (<10/cm). Yang et al. [28] have recently demonstrated that, for Eu^{3+} in 5–12 nm Y_2O_3 nanocrystals, the decay rates involving low-frequency acoustic phonons (<10/cm) are reduced by 2 orders of magnitude, whereas relaxation times for a 25/cm phonon process increase to ca. 40 ns. This is a much less pronounced effect than the μs phonon relaxation times (a 10^6 decrease in comparison with bulk) required by the 'hot-luminescence' model proposed in Refs. [17,23].

Furthermore, the energy differences observed by Yu et al. [17] between the two peaks ascribed by them to Mn^{2+} hot luminescence (viz., 540 and 660 nm) and the expected 'normal' Mn^{2+} luminescence (590 nm) is about 1500–1800/cm. To bridge this energy difference by phonon relaxation to the lowest vibrational level, coupling with the highest frequency phonons in ZnS is expected. The gap can be bridged by ~ 5 phonons of 350/cm [29]. The density of states and phonon occupation numbers of the high-energy phonons are not expected to be affected by quantum size effects or hot spots. Even though the final step in the energy dissipation process (break-up of higher energy optical phonons into low-energy acoustic phonons) may be influenced to some extent by the changes in the phonon spectrum on the low-energy side (acoustic phonons of ~ 10/cm), it is not expected that the initial relaxation from the high vibrational level in the $^4T_1$ state by emission of 4 or 5 high-energy optical phonons will be influenced to such an extent that the overall relaxation rate is reduced by a factor 10^6, considering that neither the phonon density of states of the high-energy optical phonons nor the coupling of the electronic transition on Mn^{2+} with these localized phonons will be influenced by size effects (quantum confinement of charge carriers and/or geometrical confinement of phonons). The present experiments confirm this.

This leaves the question why in Ref. [17] a very different emission spectrum was measured for Mn^{2+} in nanocrystalline ZnS. The spectra for the Mn^{2+} emission resemble, indeed, spectra that can be expected for emission from a high vibrational state, and the spectra can be nicely modelled by assuming a 10^6-fold slower phonon relaxation, as was shown in Ref. [23]. Sample and experimental differences can account for some of the discrepancies between the present results and those published in Ref. [17]. The samples investigated by Yu and co-workers [17] consisted of ZnS:Mn^{2+} nanoparticles embedded in a polymeric (polyvinyl butyral) matrix, while we investigated samples consisting of free standing aggregates of polyphosphate stabilized ZnS:Mn^{2+} nanocrystals [20]. The excitation of the samples was achieved in Ref. [17] by using an excimer laser ($\lambda_{exc} = 248$ nm, 40 ns pulse width), whereas in this work the fourth harmonic of a Nd:YAG laser was used ($\lambda_{exc} = 266$ nm, 10 ns pulse width). Although it is hard to explain the differences between the spectra in Figs. 2 and 3 in the present paper and Figs. 2 and 3 of Ref. [17], a possible explanation is saturation of the photomultiplier tube for higher intensities. The measurement of the time-resolved emission spectra relies on photon counting. In the

2 μs gate, only a limited number of counts (<200) is possible for a typical response time of a photomultiplier tube (viz., ~10 ns). If the number of detected photons increases beyond this limit (as may be the case for the centre of the Mn^{2+} emission band), the number of "counts" may actually decrease due to the fact that individual photon pulses merge together into one longer pulse, which is counted only once. For longer delays, the signal has decreased sufficiently and the "normal" Mn^{2+} spectrum is measured.

4. Conclusions

Time-resolved luminescence spectra of ZnS:Mn^{2+} nanocrystals upon 266 nm excitation were observed to consist of at least three different bands, with maxima at about 400, 460 and 590 nm. The former two bands have a fast decay time (viz., < 1 μs), and are ascribed to defect-related emission of ZnS, while the latter has a much longer decay time (ms range) and is ascribed to the $^4T_1$–$^6A_1$ emission transition of the Mn^{2+} ion.

The Mn^{2+} emission band is observed at the expected spectral energies and has a power and temperature-independent gaussian shape. The results provide no evidence of hot luminescence in ZnS:Mn^{2+} nanocrystals, regardless of the instrumental parameters (time delay and gate width), excitation density, temperature and Mn^{2+} concentration. It is concluded that there is no million-fold reduction in the phonon relaxation rates from the higher vibrational states of the $^4T_1$ excited state of Mn^{2+} in ZnS nanocrystals, in contradiction with previously reported results [17,23]. Contrary to the Mn^{2+} related emission, interesting changes are observed for the various ZnS-related emission bands as a function of excitation power and temperature.

Acknowledgements

We gratefully acknowledge the financial support of Philips Lighting NV, of the Netherlands Organization for Scientific Research (NWO) and of the Council for Chemical Sciences (CW).

References

[1] S.V. Gaponenko, Optical Properties of Semiconductor Nanocrystals, Cambridge University Press, Cambridge, 1998.
[2] L. Brus, Appl. Phys. A 53 (1991) 465.
[3] A.P. Alivisatos, J. Phys. Chem. 100 (1996) 13 226.
[4] Y. Wang, N. Herron, J. Phys. Chem. 95 (1991) 525.
[5] H. Weller, Angew. Chem. Int. Ed. Engl. 32 (1993) 41.
[6] A. Henglein, Chem. Rev. 89 (1989) 1861.
[7] R.N. Bhargava, D. Gallagher, Phys. Rev. Lett. 72 (1994) 416.
[8] R.N. Bhargava, J. Lumin. 70 (1996) 85.
[9] M. Tanaka, J. Qi, Y. Masumoto, J. Lumin. 87–89 (2000) 472.
[10] K. Sooklal, B.S. Cullum, S.M. Angel, C.J. Murphy, J. Phys. Chem. 100 (1996) 4551.
[11] H. Ito, T. Takano, T. Kuroda, F. Minami, H. Akinaga, J. Lumin. 72–74 (1997) 342.
[12] J. Yu, H. Liu, Y. Wang, F.E. Fernandez, W. Jia, L. Sun, C. Jin, D. Li, J. Liu, S. Huang, Opt. Lett. 22 (1997) 913.
[13] T.A. Kennedy, E.R. Glaser, P.B. Klein, R.N. Bhargava, Phys. Rev. B 52 (1995) 14 356.
[14] C. Jin, J. Yu, L. Sun, K. Dou, S. Hou, J. Zhao, Y. Chen, S. Huang, J. Lumin. 66/67 (1996) 315.
[15] J. Yu, H. Liu, Y. Wang, F.E. Fernandez, W. Jia, L. Sun, C. Jin, J. Liu, S. Huang, Opt. Lett. 22 (1997) 913.
[16] A.A. Bol, A. Meijerink, Phys. Rev. B 58 (1998) 15 997.
[17] J. Yu, H. Liu, Y. Wang, W. Jia, J. Lumin. 79 (1998) 191.
[18] N. Murase, R. Jagannathan, Y. Kanematsu, M. Watanabe, A. Kurita, K. Hirata, T. Yazawa, T. Kushida, J. Phys. Chem. B 103 (1999) 754.
[19] D. Gallagher, W.E. Heady, J.M. Racz, R.N. Bhargava, J. Mater. Res. 10 (1995) 870.
[20] A.A. Bol, A. Meijerink, J. Phys. Chem. B 105 (2001) 10 197.
[21] S.W. Lu, B.I. Lee, Z.L. Wang, W. Tong, B.K. Wagner, W. Park, C.J. Summers, J. Lumin. 92 (2001) 73.
[22] M. Tanaka, Y. Masumoto, Chem. Phys. Lett. 324 (2000) 249.
[23] F.G. Anderson, W.M. Dennis, G.F. Imbusch, J. Lumin. 90 (2000) 27.
[24] O. Madelung, W. Martienssen (Eds.), Landolt-Bornstein. Numerical Data and Functional Relationships in Science and Technology, Vol. III–17b, Springer, Berlin, 1988, p. 61.
[25] B.D. Cullity, Elements of X-ray Diffraction, Addison-Wesley, Reading, MA, 1978, p. 102.
[26] D. Gallagher, W.E. Heady, J.M. Racz, R.N. Bhargava, J. Crystal Growth 138 (1994) 970.
[27] A. van Dijken, A.H. Janssen, M.H.P. Smitsmans, D. Vanmaekelbergh, A. Meijerink, Chem. Mater. 10 (1998) 3513.
[28] H.S. Yang, K.S. Hong, S.P. Feofilov, B.M. Tissue, R.S. Meltzer, W.M. Dennis, J. Lumin. 83–84 (1999) 139.
[29] A. Anastassiadou, E. Liarocapis, E. Anastassakis, Solid State Commun. 69 (1988) 157.